


Cathepsin B Relocalization in Late Membrane Disrupted Neurons Following Diffuse Brain Injury in Rats

ASN Neuro
Volume 14: 1–14
© The Author(s) 2022
Article reuse guidelines:
sagepub.com/journals-permissions
DOI: 10.1177/17590914221099112
journals.sagepub.com/home/asn


Martina L. Hernandez¹ , Michael Marone², Karen M. Gorse¹
and Audrey D. Lafrenaye¹

Abstract

Traumatic brain injury (TBI) has consequences that last for years following injury. While TBI can precipitate a variety of diffuse pathologies, the mechanisms involved in injury-induced neuronal membrane disruption remain elusive. The lysosomal cysteine protease, Cathepsin B (Cath B), and specifically its redistribution into the cytosol has been implicated in cell death. Little is known about Cath B or neuronal membrane disruption chronically following diffuse TBI. Therefore, the current study evaluated Cath B and diffuse neuronal membrane disruption over a more chronic post-injury window (6 h–4 w). We evaluated Cath B in adult male Sprague-Dawley rats following central fluid percussion injury (CFPI). Expression of Cath B, as well as Cath B-associated pro (Bak and AIF) and anti-apoptotic (Bcl-xl) proteins, were assessed using western blot analysis. Cath B activity was also assessed. Localization of Cath B was evaluated in the membrane disrupted and non-disrupted population following CFPI using immunohistochemistry paired with quantitative image analysis and ultrastructural verification. There was no difference in expression or activity of Cath B or any of the associated proteins between sham and CFPI at any time post-injury. Immunohistological studies, however, showed a sub-cellular re-localization of Cath B at 2 w and 4 w post-injury in the membrane disrupted neuronal population as compared to the time-point matched non-disrupted neurons. Both membrane disruption and Cath B relocalization appear linked to neuronal atrophy. These observations are indicative of a late secondary pathology that represents an opportunity for therapeutic treatment of these neurons following diffuse TBI.

Summary Statement Lysosomal cathepsin B relocates to the cytosol in neurons with disrupted plasmalemmal membranes weeks following diffuse brain injury. Both the membrane disrupted and cathepsin B relocalized neuronal subpopulations displayed smaller soma and nucleus size compared to non-pathological neurons, indicating atrophy.

Keywords

cathepsin B, membrane disruption, traumatic brain injury, neuronal atrophy, Bak/Bcl-XL, AIF

Received January 26, 2022; Revised April 13, 2022; Accepted for publication April 20, 2022

Introduction

Traumatic brain injury (TBI) affects at least 2.8 million people in the US every year as of 2017, and the cost of TBI related-hospital admissions as of 2016 was estimated to be \$21 billion per year and rising (Marin et al., 2017; Taylor et al., 2017). The main event is not isolated, as TBI patients experience chronic symptoms due to secondary diffuse pathology throughout the brain (McMahon et al., 2014). This diffuse pathology is often hard to find on radiological and medical imaging and is relatively understudied compared to focal pathology, which has been highly characterized pre-clinically and clinically.

Neuronal membrane disruption has been found in various TBI models both in vitro and in vivo and in rodents and swine models (Hernandez et al., 2019; Keating et al., 2020; LaPlaca et al., 2019; Prado and LaPlaca, 2020; Ryu et al., 2021). A

¹Anatomy and Neurobiology, Virginia Commonwealth University, Richmond, Virginia, USA

²Pharmacology and Toxicology, Virginia Commonwealth University, Richmond, Virginia, USA

Corresponding Author:

Audrey D. Lafrenaye, Department of Anatomy and Neurobiology, Box 980709, Richmond, VA 23298, USA.
Email: audrey.lafrenaye@vcuhealth.org



study found that neuronal membrane disruption presents 6 h to 4 w in a biphasic manner (Hernandez et al., 2019). They documented acute membrane disruption following injury at 6 h, 1d, 3d, then decreasing at 1 w. However, at 2 w and 4 w, we see a resurgence of the membrane disrupted population indicative of a secondary pathology occurring late that extends beyond the mechanical damage immediately seen post-injury. The reemergence of membrane disruption at late time points has an unknown etiology. Earlier studies honed onto a molecular mechanism for sub-acute membrane disruption driven by Cathepsin B (Cath B), however it is not known if this continues at later time points (Lafrenaye et al., 2012).

Cath B is a ubiquitously expressed lysosomal cysteine protease that performs regulatory functions such as recycling and breakdown of intramembrane proteins and cleavage of precursor proteins (Cavallo-Medved et al., 2011). However, Cath B has also been implicated in cell death, autophagy and various other cell-damage pathways (Boya et al., 2003; Chaitanya and Babu, 2008; Chowdhury et al., 2019; de Castro et al., 2016; Foghsgaard et al., 2001; Mollan et al., 2016; Nagakannan et al., 2021; Oberle et al., 2010). Cath B has been previously shown to mediate cell death via lysosomal membrane permeabilization. This pathway appears to evolve in multiple ways; either via cleavage of B-cell lymphoma 2 (Bcl-2)/Bcl-XL, pro-survival proteins, which in turn releases the pro-apoptotic proteins Bak/Bax, that then enter the mitochondria to release cytochrome C leading to cell damage/death or via direct interaction of Cath B with apoptosis initiating factor (AIF) which goes to the mitochondria to induce the apoptotic cascade (Boya et al., 2003; Chaitanya and Babu, 2008; Oberle et al., 2010; Chowdhury et al., 2019). While Cath B usually functions within the acidic environment of the lysosome, it also has endopeptidase activity at the more neutral pH of the cytosol, unlike other lysosomal proteases. Within the context of TBI, Cath B has been found to be upregulated in rodent TBI models of focal lesions, such as the controlled cortical impact (CCI) and penetrating ballistic-like brain injury (PBBI) (Luo et al., 2010; Hook et al., 2013; Boutté et al., 2020). Additional findings within patient cerebrospinal fluid also indicated an upregulation of Cath B within hours or days post-penetrating TBI compared to non-TBI controls, providing further evidence that Cath B could play a role in TBI pathology (Boutté et al., 2020). Another study presented that Cath B was re-localized from the lysosome and into the cytosol at 6 h post-central fluid percussion injury (CFPI) and secondary elevations of intracranial pressure (Lafrenaye et al., 2012). However, potential changes in Cath B throughout the progression of diffuse injury remain elusive, specifically at later time points where it could be a driving molecular mechanism for sub-acute/chronic diffuse membrane disruption.

We, therefore, explored Cath B in the context of protein expression and activity in rats from 6 h to 4 w post-CFPI. We also evaluated proteins involved in both of the Cath

B-mediated cell damage pathways, Bak, Bcl-XL, and AIF via western blot. Protein analyses were followed by a microscopic exploration of subcellular localization of Cath B throughout the post-injury time course. Finally, we assessed indications of cellular and nuclear atrophy in relation to membrane disruption and Cath B re-localization. The findings reported below underline that the role of Cath B following TBI may be more variable with pathological presentations of diffuse TBI compared to focal TBI.

Materials and Methods

Animals

Experiments were conducted using protocols in accordance with the Virginia Commonwealth University institutional ethical guidelines concerning the care and use of laboratory animals (Institutional Animal Care and Use Committee, Virginia Commonwealth University), which adhere to regulations including, but not limited to, those set forth in the Guide for the Care and Use of Laboratory Animals, 8th Edition (National Research Council). Animals were housed in individual cages on a 12 h light-dark cycle with free access to food and water. Archived tissue and homogenates from our previous study using adult male Sprague-Dawley rats, $n = 57$ weighing 350–450 g, were used for this study (Hernandez et al., 2019). Our a priori exclusion criteria included weight loss of more than 20% of their pre-injury body weight or gross brain pathology (contusion, subdural hematoma, or gross tissue loss). No animals met exclusion criteria in this study. Animal injury state and survival timepoint were randomly determined using a random number generator on the day of surgery. All surgeries were conducted by the same surgeon during the same times of day to reduce variability.

Surgical Preparation and Injury Induction

Corresponding to Hernandez et al. (2019), Animals were anesthetized with 4% isoflurane in 30% O₂ and 70% N₂O then intubated and ventilated with 2% isoflurane in 30% O₂ and 70% N₂O throughout the duration of the surgery, injury, and post-injury physiological monitoring. Heart rate, respiratory rate, and blood oxygenation were monitored via a hind-paw pulse oximetry sensor (STARR Life Sciences, Oakmont, PA) for the duration of anesthesia, except during the induction of injury. Body temperature was maintained at 37°C with a rectal thermometer connected to a feedback-controlled heating pad (Harvard Apparatus, Holliston, MA). All animals were placed in a stereotaxic frame (David Kopf Instruments, Tujunga, CA). A midline incision was made, and a 4.8 mm circular craniectomy was made along the sagittal suture midway between bregma and lambda for injury induction. A 2 mm burr hole was also drilled in the left parietal bone overlying the left lateral ventricle (0.8 mm posterior,

1.3 mm lateral, and 2.5–3 mm ventral to bregma) through which a 25-gauge needle, connected to a pressure transducer and microinfusion pump (11 Elite syringe pump; Harvard Apparatus) via sterile saline-filled PE50 tubing, was placed into the left lateral ventricle. Appropriate placement was verified via a 1.3 μ l/min infusion of sterile saline within the closed fluid-pressure system during needle placement. The needle was held in the ventricle for at least 5 min to record pre-injury intracranial pressure (ICP). After the 5-min reading, the needle was slowly removed, and the burr hole was covered with bone wax before preparation for sham or CFPI (Dixon et al., 1987; Lafrenaye et al., 2014). Briefly, a Leur-Loc syringe hub was affixed to the craniectomy site, and dental acrylic (methyl-methacrylate; Hygenic Corp., Akron, OH) was applied around the hub and allowed to harden. Anesthetized animals were removed from the stereotaxic frame and injured at a magnitude of 2.05 ± 0.15 atmospheres and duration of ~ 22 msec. The pressure pulse was measured by a transducer affixed to the injury device and displayed on an oscilloscope (Tektronix, Beaverton, OR). Immediately after the injury, the animal was reconnected to the ventilator and physiologic monitoring device and the hub and dental acrylic were removed en bloc. Gelfoam was placed over the craniectomy/injury site, and the scalp was sutured. The animal was then replaced in the stereotaxic device, and the ICP probe was reinserted into the lateral ventricle, as described above, for post-injury ICP monitoring. The animals were then allowed to recover and were returned to clean home cages. Identical surgical procedures were followed for sham-injured animals, without release of the pendulum to induce injury (Hernandez et al., 2019).

Tracer Infusion

Two hours prior to sacrifice, tagged dextran (40 mg/ml in sterile 0.9% saline; ~ 1.6 mg/kg) was infused into the lateral ventricle as described (Lafrenaye et al., 2012; Hernandez et al., 2019). Briefly, 15 μ l of 10 kDa dextran conjugated to either 488-Alexa Fluor (Cat#: D22910, Invitrogen, Carlsbad, CA), 568-Alexa-Fluor (Cat#: D22912; Invitrogen, Carlsbad, CA), or biotin (Cat#: D1956; Invitrogen, Carlsbad, CA) was infused into the left lateral ventricle at 0.5–1.3 μ l/min, with continuous ICP monitoring. To avoid bias caused by differences in fluorescent signal detectability, animals were randomly assigned a tag (Alexa 488, Alexa 568 or biotin). The tracer was allowed to diffuse throughout the parenchyma for 2 h prior to transcardial perfusion at 6 h, 1d, 3d, 1w, 2w, or 4w post-sham or CFPI.

Tissue Processing

At appropriate time-points between 6 h and 4w post-injury, the animals were injected with 150 mg/kg euthanasia-III solution (Henry Schein, Dublin, OH), then underwent transcardial perfusion with cold 0.9% saline. Lateral neocortices were dissected from the right hemisphere of the brain and

frozen for assessments of protein expression and activity followed by a switch in transcardial perfusate to 4% paraformaldehyde/0.2% glutaraldehyde in Millonig's buffer (136 mM sodium phosphate monobasic/109 mM sodium hydroxide) to fix the left side of the brain for subsequent immunohistochemical or electron microscopic (EM) processing and analysis. After transcardial perfusion, the brains were removed, post-fixed for 24–48 h, then sectioned coronally in 0.1 M phosphate buffer with a vibratome (Leica, Banockburn, IL) at a thickness of 40 μ m from bregma to 4.0 mm posterior to bregma. Sections were collected serially in 12 well-plates and stored in Millonig's buffer at 4°C. A random starting well (wells 1–12) was selected using a random number generator and four serial sections (each 480 μ m apart) were used for histological analyses. All histological analyses were restricted to layers V and VI of the lateral somatosensory neocortex extending from the area lateral to CA1 to the area lateral to CA3 of the hippocampus (Hernandez et al., 2019).

Western Blotting

As performed in Hernandez et al. (2019), lateral neocortices of sham $n=6$ ($n=1$ /time point) and TBI rats $n=6$ /time point were homogenized in NP40 Buffer (150 mM NaCl, 50 mM Tris pH 8.0, 1% Triton) and protease inhibitor cocktail (AEBSF 10.4 mM, Aprotinin 8 μ M, Bestatin 400 μ M, E-64 140 μ M, Leupeptin 8 μ M, Pepstatin A 150 μ M, Cat#: P8340, Sigma, Saint Louis, MO). Protein concentrations were measured using a NanoDrop Lite (Thermo Fisher Scientific, Wilmington, DE). Protein (20 μ g for Cathepsin B, 10 μ g Bak, Bcl-XL, and AIF) was boiled for 10 min in 50 mM dithiothreitol (Cat#: 1610610; Bio-Rad; Hercules, CA), 2x Laemmli loading buffer (Cat#: 1610737; Bio-Rad; Hercules, CA) and run at 200 Volts for 30 min on Mini-PROTEAN TGX Stain-Free 4–20% precast polyacrylamide gels (Cat#: 4568096; Bio-Rad, Hercules, CA). Protein was transferred onto 0.45 μ m PVDF membranes using a Bio-Rad Transblot Turbo transfer system set to the mixed molecular weight manufacturer setting (1.3–2.5 Amps, 25 Volts for 7 min). Western blotting was done on an iBind flex apparatus (Invitrogen, Carlsbad, CA) using primary antibodies rabbit anti-Cathepsin B (1:1000; Cat#: 31718, RRID:AB_2687580), rabbit anti-Bak (1:1000; Cat#: 12105, RRID:AB_2716685), rabbit anti-Bcl-xl (1:1000; Cat#: 2764, RRID:AB_2228008) or rabbit anti-AIF (1:1000; Cat#: 5318, RRID:AB_10634755) (Cell Signaling Technology, Danvers, MA) and anti-rabbit-HRP secondary antibody (1:5000; Cat#: 111-035-003; Jackson ImmunoResearch Laboratories, West Grove, PA, RRID:AB_2313567). Total protein (Stain Free) and chemiluminescent images were taken on a ChemiDoc imaging system (BioRad). Densitometric analyses of Cathepsin B, AIF, Bak, and Bcl-XL were performed in ImageJ (National Institutes of Health; Bethesda, MD). Cathepsin B, AIF, Bak and Bcl-XL protein bands were normalized to total protein and sham controls. Additionally, the ratio of normalized Bak and Bcl-XL was calculated. All western blots

were run in triplicates on three separate gels to reduce run-to-run variability biasing the results. A negative control was also done to verify band specificity (Supplementary Figure 1).

Cellular Cathepsin B Localization Analysis

Fluorescently tagged dextran-containing cells, indicative of membrane disruption, could be visualized via confocal microscopy without further processing, however, biotin-conjugated dextran required immunolabeling for visualization. Two tissue sections/animal from 6 h (n=5), 1d (n=5), 3d (n=4) 1w (n=5), 2w (n=5), 4w (n=5) were blocked with 5% normal goat serum (NGS) or 5% normal horse serum (NHS), 2% bovine serum albumin (BSA), and permeabilized with 1.5% triton-X for 2 h. This was followed by immunolabeling using primary antibodies rabbit anti-Cathepsin B (1:700; Cat#: 31718 Cell Signaling Technology, Danvers, MA, RRID:AB_2687580) and Goat anti-biotin (1:2000; Cat#: 31852; Thermo Scientific, Rockford, IL, RRID:AB_228243) as needed for animals infused with biotin-conjugated dextrans. Tissue was incubated in secondary antibodies Alexa-633 conjugated goat anti-rabbit(1:700; Cat#: A21070; Life Technologies, Carlsbad, CA, RRID:AB_2535731) and Alexa-488 conjugated donkey anti-goat (1:700; Cat#: A11055; Life Technologies, Carlsbad, CA, RRID:AB_2534102) and the tissue was mounted onto slides using Vectashield hardset mounting medium with 4',6-diamidino-2-phenylindole (DAPI) (Cat#: H-1500; Vector Laboratories, Burlingame, CA). Quantitative analysis was performed as described previously (Lafrenaye et al., 2012; Hernandez et al., 2019). Briefly, 4 confocal images each section; 2 sections/animal of the left neocortical region of interest were taken at 40x magnification using a Zeiss LSM 710 System (Carl Zeiss) in a systematically random fashion by an investigator blinded to animal group using the dextran tag to verify images included neurons with and without membrane disruption. Image acquisition settings were held constant for comparable regions (layer V or VI) and dextran (488-tagged, 568-tagged or biotin-tagged) for all groups analyzed. Equal numbers of membrane disrupted, and non-disrupted neurons were randomly selected in each image. The cell body and nucleus of all neurons assessed were traced and the area of the soma and nucleus were quantified via the measure tool in FIJI (ImageJ). Localization (either punctate or diffuse) of Cathepsin B was assessed for each neuron by eye using the traces and without seeing the dextran labeling. Membrane disrupted and non-disrupted neurons were randomized for each image to reduce investigator bias during assessment of Cathepsin B localization. The localization of Cathepsin B was expressed as a percentage of neurons demonstrating punctate (lysosomal) Cathepsin B localization of the total membrane disrupted or non-disruption neuronal population assessed at each time point (6 h–4w). In addition, somal and nuclear size were assessed for both membrane disruption (membrane

disrupted vs. non-disrupted) and Cathepsin B localization (punctate vs. diffuse localization) subpopulations at each time point (6 h–4w).

Quantification of Cathepsin B Activity

Portions of the dissected right lateral neocortices of 6 h–4w sham and injured animals were homogenized in 50 μ M citric acid at a pH 6.0, spun at 12,000 \times g at 4° C for 10 min and the supernatant of the whole homogenate was collected. Protein concentrations were measured using a NanoDrop Lite (Thermo Fisher Scientific, Wilmington, DE) and Cathepsin B activity was measured in a 96-well plate, each well containing 2x Assay Buffer (100 mM sodium acetate pH 5.5, 2 mM EDTA, 200 mM sodium chloride, 8 mM DTT), 2 μ g of neocortex whole homogenate, and Z-Phe-Arg-7-amino-4-(trifluoromethyl) coumarin (ZFR-AMC), a substrate for cysteine proteases that fluoresces upon cleavage by Cathepsin B (Hook et al., 2013; Boutté et al., 2020; Yoon et al., 2021). Assay specificity for Cathepsin B was validated using Cathepsin B specific inhibitor, CA-074, and general cysteine protease inhibitor, E64c, pre-incubated in brain homogenate (Supplementary Figure 2). The plate was read 30- and 60-min post-substrate addition at 365/450 nm excitation/emission. Each sample was loaded in triplicate per plate for three independent runs to reduced pipetting and run-to-run variability biasing the results. A positive control well with purified human liver Cathepsin B 5 ng and a negative control well with only assay buffer and substrate were included in every run.

Ultrastructural Assessment of Cathepsin B Localization

In preparation for electron microscopic (EM) analysis, tissue was labeled with rabbit antibodies targeted to Cathepsin B (1:500; Cat#: 31718 Cell Signaling Technology, Danvers, MA). Tissue slices were then blocked with 5% NGS, followed by incubation with biotinylated goat anti-rabbit (1:1000; Cat#: BA-5000; Vector Laboratories) secondary antibody. Sections were incubated in avidin biotinylated enzyme complex using the Vectastain ABC kit (Vector Laboratories) followed by visualization with diaminobenzidine (DAB) in 0.1 M phosphate buffer. Tissue sections were osmicated, dehydrated, and embedded in epoxy resin on plastic slides as published (Hernandez et al., 2019). After resin curing, areas in the lateral neocortex within layers V and VI that contained adequate Cathepsin B labeling and in regions approximate to locations of membrane disruption were identified using light microscopy. These areas were removed, mounted on plastic studs, and 70 nm sections were cut and mounted on Formvar-coated slotted grids. The grids were stained in 5% uranyl acetate in 50% methanol and 0.5% lead citrate. Electron micrographs were imaged using a JEOL JEM 1230 transmission electron microscope equipped with an Orius SC1000 CCD camera (Gatan, Pleasanton, CA). Every neuron within each grid, 3 grids total, n=2 animals, 1 grid for 1 animal and 2 grids for the

other, were imaged and all images were qualitatively assessed for distribution of Cathepsin B within or in approximation to the lysosomal compartment.

Statistical Analysis

Data were tested for normality prior to utilizing parametric or non-parametric assessments, which were conducted using SPSS (IBM Corporation, Armonk, NY) software. Animal numbers for each group were determined by an a priori power analysis using effect size and variability previously observed in the lab when assessing pathology between sham and injured groups using the CFPI model, an $\alpha = 0.05$, and a power of 80%. Two-way or one-way analysis of variance (ANOVA) and Bonferroni post hoc tests were performed for all between-group analyses. Statistical significance was set to $p < 0.05$. Data are presented as mean \pm standard error of the mean (SEM).

Results

Protein Expression of Cathepsin B or its Proteolytic Activity was Unchanged Following CFPI

The overall expression of Cath B within the lateral neocortex was evaluated for changes following CFPI throughout the 6 h to 4w post-injury time course. Western blot analysis revealed that Cath B protein levels were not significantly different for sham animals ($100.91 \pm 4.85\%$) and TBI animals at 6 h ($87.27 \pm 4.53\%$ of sham), 1d ($85.93 \pm 4.84\%$ of sham), 3d ($110.24 \pm 14.49\%$ of sham), 1w ($83.48 \pm 5.03\%$ of sham), 2w ($100.86 \pm 8.79\%$ of sham), and 4w ($105.25 \pm 10.88\%$ of sham) post-CFPI (Figure 1A and B; one-way ANOVA $F_{6, 35} = 1.527$, $p = 0.198$).

Cath B has been implicated in various cell damage pathways. One of these pathways involved AIF, which is cleaved by cathepsins from the mitochondria to set forth cell death (Chaitanya and Babu, 2008; Chowdhury et al., 2019). Additionally, Cath B can cleave Bcl-XL, a pro-survival protein that interacts with Bak, a pro-apoptotic protein which advances cell death by release of cytochrome C (Boya et al., 2003; Oberle et al., 2010). Therefore, the protein expression of AIF as well as the expression ratio of the antagonizing proteins Bcl-XL and Bak were also assessed over the 4w time course following injury. The quantity of AIF following CFPI at 6 h ($96.16 \pm 9.47\%$ of sham), 1d ($87.61 \pm 8.08\%$ of sham), 3d ($87.88 \pm 6.63\%$ of sham), 1w ($85.24 \pm 11.57\%$ of sham), 2w ($98.93 \pm 10.37\%$ sham), 4w ($102.18 \pm 10.65\%$ of sham) was comparable to AIF levels in the lateral neocortex of sham controls ($100 \pm 0.36\%$; Figure 1C and D; one-way ANOVA $F_{6,35} = 0.604$, $p = 0.725$). There was also no difference in the Bak/Bcl-XL expression ratio between sham (101.66 ± 3.85) and TBI animals at 6 h (101.06 ± 22.66), 1d (97.70 ± 9.36), 3d (98.76 ± 12.73), 1w (101.05 ± 13.02), 2w (107.77 ± 7.62),

and 4w (101.35 ± 7.62 ; Figure 1E and F; one-way ANOVA $F_{6,35} = 0.069$, $p = 0.999$).

Whereas most Cathepsins are active at the lower pH of the lysosomes, Cath B is also active at more neutral pHs, such as that of the cytosol (Nägler et al., 1997; Khouri et al., 1991; Ruzza et al., 2006). Therefore, the question arose regarding Cath B's localization and proteolytic activity over time following CFPI. Proteolytic activity of Cath B was not significantly different between sham animals ($99.81 \pm 9.99\%$) and TBI animals at 6 h ($100.25 \pm 9.08\%$ of sham), 1d ($92.57 \pm 12.16\%$ of sham), 3d ($119.24 \pm 14.86\%$ of sham), 1w ($90.50 \pm 5.03\%$ of sham), 2w ($103.59 \pm 17.08\%$ of sham), and 4w ($125.01 \pm 25.60\%$ of sham) post-CFPI (one-way ANOVA $F_{6, 23} = 0.753$, $p = 0.614$; Figure 2).

Cathepsin B re-Localizes from Lysosomes to Cytosol in Disrupted Neurons at 2 and 4 Weeks Following Central Fluid Percussion Injury

The re-localization/redistribution of Cath B from the lysosome to the cytosol has been associated with pathological progression (Windelborn and Lipton, 2008; Kilinc et al., 2010; Oberle et al., 2010). Additionally, there is redistribution of Cath B in acutely membrane disrupted neurons of rats sustaining TBI and secondary ICP elevations (Lafrenaye et al., 2012). However, to our knowledge, Cath B localization has not been rigorously assessed in later stages of neuronal membrane disrupted populations following diffuse TBI alone. Therefore, Cath B localization was determined as punctate (intra-lysosomal) or diffuse (extra-lysosomal) for both membrane disrupted and non-disrupted neurons in the injured lateral neocortex throughout the time course from 6 h–4w post-CFPI (Figure 3A). Sham animals were not included in this assessment as they have no discernable membrane disruption (Hernandez et al., 2019), thus would provide no further information about the membrane disrupted population in relation to Cath B localization. Cath B was found to be localized within puncta in non-disrupted neurons at 6 h ($72.88 \pm 3.72\%$), 1d ($63.91 \pm 4.18\%$), 3d ($77.88 \pm 4.09\%$), 1w ($80.73 \pm 3.79\%$), 2w ($80.52 \pm 3.20\%$), 4w ($87.22 \pm 2.91\%$), post-CFPI. The majority of Cath B was also localized within lysosomal puncta in disrupted neurons at 6 h ($86.99 \pm 2.79\%$) $p = 0.425$, 1d ($50.34 \pm 4.11\%$) $p = 0.636$, 3d ($66.99 \pm 4.66\%$) $p = 1.00$, 1w ($65.63 \pm 4.21\%$) $p = 0.552$, however, there was a significant reduction in the percentage of membrane disrupted neurons demonstrating punctate localization of Cath B at 2w ($43.84 \pm 4.66\%$) $p = 4.88 \times 10^{-11}$, and 4w ($32.35 \pm 4.66\%$) $p = 5.34 \times 10^{-19}$ post-CFPI (Figure 3B, one-way ANOVA; $F_{11,1539} = 19.88$, $p = 6.6 \times 10^{-38}$).

The percentages of neurons demonstrating punctate Cath B indicated an effect of membrane disruption (two-way ANOVA; $F_{1,1539} = 74.83$, $p = 1.27 \times 10^{-17}$) and time (two-way ANOVA; $F_{5,1539} = 11.42$, $p = 7.73 \times 10^{-11}$) on Cath B re-localization. There were also significant interactions between neuronal membrane disruption and time on

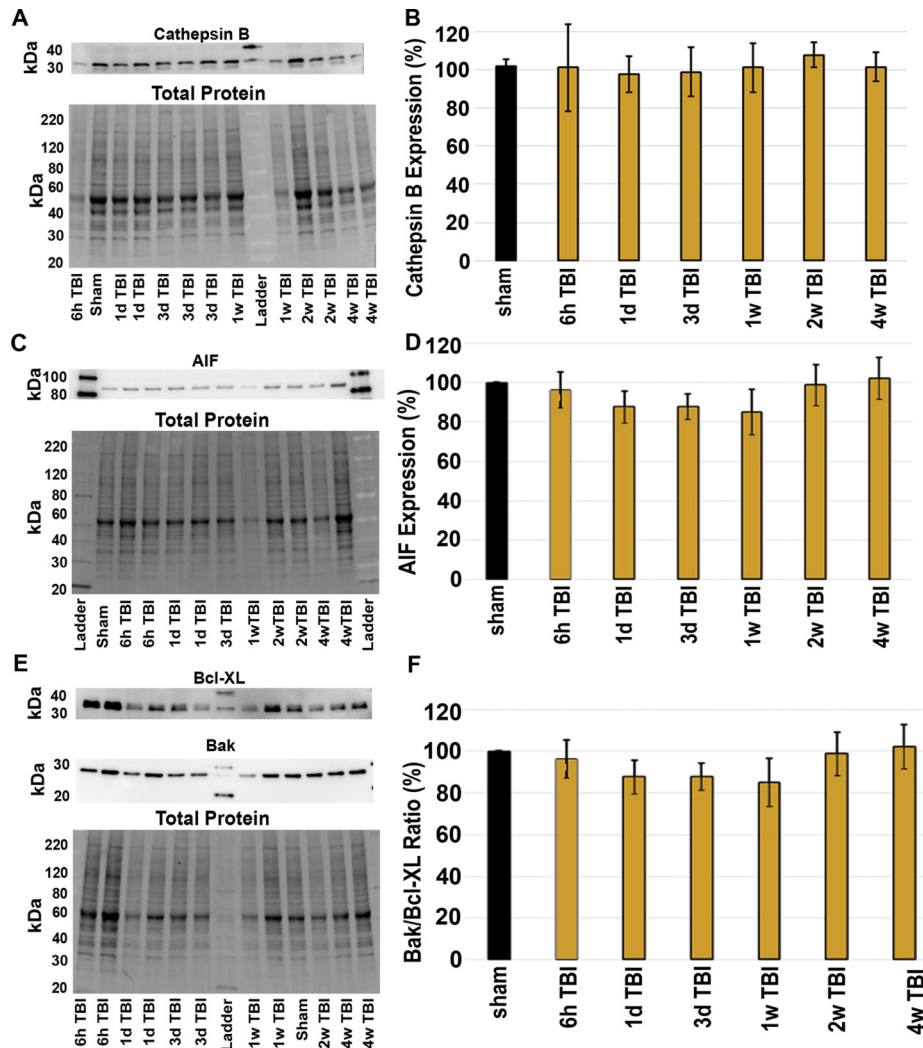


Figure 1. There were no differences in the expression of Cathespin B (Cath-B) or Cath-B signaling proteins 6 h to 4w post-CFPI compared to sham. (A) representative chemiluminescent western blots depicting (A) Cath-B protein bands at 24/27 kDa, (C) AIF protein bands at ~67 kDa, as well as (E) Bcl-XL and Bak protein bands at 30 and 25 kDa, respectively, from homogenized lateral cortices. All westerns were normalized to total protein as depicted below the corresponding western blot. Bar graphs depicting the averaged normalized protein expression of (B) Cath-B, (D) AIF, and (F) the expression ratio of Bcl-XL/Bak in sham animals ($n = 6$) [black bars] and at 6 h–4w post-injury in TBI animals [yellow bars] ($n = 6$ /time point). There were no differences in the expression of any proteins assessed following CFPI compared to sham. Mean \pm S.E.M.

Cath B localization (two-way ANOVA; $F_{5,1539} = 19.02$, $p = 2.12 \times 10^{-18}$).

Ultrastructural qualitative analysis of neurons with immunoelectron microscopy was used to further scrutinize subcellular localization of Cath B, in particular, that the diffuse distribution of Cath B that we saw in the confocal micrographs was indeed indicative of Cath B redistributing out of the lysosomal compartment. While we did observe immunolabeled Cath B completely contained within the lysosomal domain in neurons 6 h–4w following CFPI (Figure 4A), a majority of the neurons analyzed demonstrated some degree of Cath B redistribution outside of the lysosome (Figure 5B and C). This redistribution of Cath B was observed in many

of the neurons assessed within the lateral neocortex at 2w and 4w. These data support our confocal findings of Cath B re-localization from the lysosome into the cytosol at 2 and 4w post-CFPI.

Cathespin B re-Localization and Neuronal Membrane Disruption are Associated with Reductions in Cellular and Nuclear Area

As diffuse neuronal injuries following TBI have been shown to precipitate cellular changes, such as atrophy, without leading to cell death (Lifshitz et al., 2007; Greer et al., 2011), we measured the somal and nuclear area of membrane

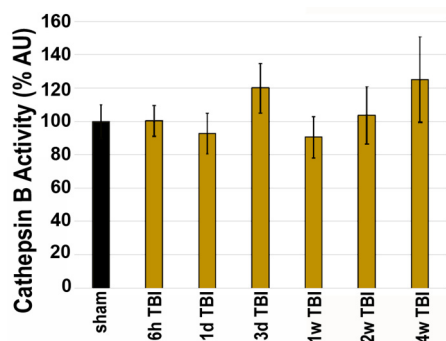


Figure 2. Cathepsin B activity does not significantly change following injury. Normalized average fluorescence intensity of Cathepsin B activity within whole homogenates of the lateral neocortex is reported in the bar graph. Sham animal ($n=5$) [black bars] (black bar) Cathepsin B activity was not found to be different from 6 h–4w post-CFPI (yellow bar; $n=4$ / time point) reported as mean \pm S.E.M.

disrupted and non-disrupted neurons and neurons demonstrating punctate or diffuse Cath B localization within the lateral neocortex of the injured brain 6 h–4w post-CFPI. The mean somal areas of non-disrupted neurons at 6 h–4w post-CFPI were approximately $126 \mu\text{m}^2$; 6 h ($131.11 \pm 3.28 \mu\text{m}^2$), 1d ($118.31 \pm 3.02 \mu\text{m}^2$), 3d ($133.00 \pm 2.76 \mu\text{m}^2$), 1w ($128.61 \pm 3.15 \mu\text{m}^2$), 2w ($110.60 \pm 3.15 \mu\text{m}^2$), and 4w ($134.31 \pm 3.49 \mu\text{m}^2$). The mean somal areas of membrane disrupted neurons from 6h–4w post-CFPI were approximately $108 \mu\text{m}^2$: 6 h ($108.90 \pm 4.29 \mu\text{m}^2$) $p=3.16 \times 10^{-4}$, 1d ($109.25 \pm 3.24 \mu\text{m}^2$) $p=1.00$, 3d ($128.63 \pm 4.25 \mu\text{m}^2$) $p=1.00$, 1w ($125.49 \pm 5.54 \mu\text{m}^2$) $p=1.00$, 2w ($80.35 \pm 2.73 \mu\text{m}^2$) $p=1.80 \times 10^{-8}$, and 4w ($92.65 \pm 3.37 \mu\text{m}^2$) $p=1.85 \times 10^{-12}$ (Figure 5A, one-way ANOVA; $F_{11,1539}=22.13$, $p=2.12 \times 10^{-42}$). There was a significant decrease in somal area of membrane disrupted neurons at 6 h, 2w and 4w post-injury.

Somal area had main effects on time (two-way ANOVA; $F_{5,1539}=75.923$, $p=8.79 \times 10^{-24}$) and membrane disruption (two-way ANOVA; $F_{1,1539}=24.479$, $p=7.48 \times 10^{-18}$). There was a significant interaction between membrane disruption and time on somal area (two-way ANOVA; $F_{5,1539}=8.568$, $p=5.12 \times 10^{-8}$).

The mean nucleus area of non-disrupted neurons 6 h–4w post-CFPI were approximately $79 \mu\text{m}^2$; 6 h ($85.40 \pm 1.98 \mu\text{m}^2$), 1d ($78.20 \pm 1.75 \mu\text{m}^2$), 3d ($83.75 \pm 2.10 \mu\text{m}^2$), 1w ($76.11 \pm 2.17 \mu\text{m}^2$), 2w ($67.55 \pm 1.74 \mu\text{m}^2$), and 4w ($82.21 \pm 2.04 \mu\text{m}^2$). The mean nucleus area of disrupted neurons 6h–4w post-CFPI were approximately $60 \mu\text{m}^2$; 6 h ($53.62 \pm 2.42 \mu\text{m}^2$) $p=1.64 \times 10^{-27}$, 1d ($67.86 \pm 1.82 \mu\text{m}^2$) $p=0.027$, 3d ($75.56 \pm 2.51 \mu\text{m}^2$) $p=1.00$, 1w ($73.46 \pm 3.33 \mu\text{m}^2$) $p=1.00$, 2w ($43.70 \pm 2.00 \mu\text{m}^2$) $p=2.22 \times 10^{-11}$, 4w ($44.79 \pm 2.38 \mu\text{m}^2$) $p=7.47 \times 10^{-25}$, (Figure 5B, one-way ANOVA; $F_{11,1303}=37.92$, $p=4.12 \times 10^{-71}$). It was noted that membrane disrupted neurons 6 h, 1d, 2w and

4w demonstrated significant reduction in nucleus area compared to non-disrupted neurons at the same timepoints.

Nucleus area had main effects from membrane disruption (two-way ANOVA; $F_{1,1303}=213.312$, $p=7.43 \times 10^{-45}$) and time (two-way ANOVA; $F_{5,1303}=27.379$, $p=2.03 \times 10^{-26}$). This data set was probed with a two-way ANOVA that highlights an interaction of membrane disruption and time on nucleus area (two-way ANOVA; $F_{5,1303}=19.064$, $p=2.43 \times 10^{-18}$).

When assessing somal area of neurons based on Cath B localization, we found that at 6 h–4w cortical neurons demonstrating punctate localization were approximately $127 \mu\text{m}^2$; 6 h ($121.61 \pm 3.17 \mu\text{m}^2$), 1d ($124.12 \pm 3.11 \mu\text{m}^2$), 3d ($136.64 \pm 2.80 \mu\text{m}^2$), 1w ($136.80 \pm 3.72 \mu\text{m}^2$), 2w ($110.68 \pm 2.77 \mu\text{m}^2$) and 4w ($129.46 \pm 3.54 \mu\text{m}^2$) (Figure 5C). This was in contrast to the somal area of diffuse Cath B localization neurons that was approximately $99 \mu\text{m}^2$; 6 h ($113.21 \pm 5.69 \mu\text{m}^2$) $p=1.00$, 1d ($99.63 \pm 2.73 \mu\text{m}^2$) $p=3.50 \times 10^{-5}$, 3d ($115.51 \pm 4.96 \mu\text{m}^2$) $p=0.053$, 1w ($100.79 \pm 5.98 \mu\text{m}^2$) $p=8.09 \times 10^{-8}$, 2w ($71.04 \pm 2.54 \mu\text{m}^2$) $p=3.09 \times 10^{-14}$, and 4w ($93.29 \pm 3.35 \mu\text{m}^2$) $p=3.68 \times 10^{-9}$. (Figure 5C, one-way ANOVA; $F_{11,1539}=28.189$, $p=2.86 \times 10^{-54}$).

Somal area had main effects from Cath B localization (two-way ANOVA; $F_{1,1539}=147.413$, $p=1.84 \times 10^{-32}$) and time (two-way ANOVA; $F_{5,1539}=20.87$, $p=3.16 \times 10^{-20}$). An interaction of time and Cath b localization on somal area was found (two-way ANOVA; $F_{5,1539}=4.483$, $p=4.64 \times 10^{-4}$).

When assessing nucleus area of neurons based on Cath B localization, we found that at 6 h–4w cortical neurons demonstrating punctate localization were approximately $77 \mu\text{m}^2$; 6 h ($69.39 \pm 2.14 \mu\text{m}^2$), 1d ($77.84 \pm 1.76 \mu\text{m}^2$), 3d ($84.13 \pm 1.58 \mu\text{m}^2$), 1w ($81.80 \pm 1.94 \mu\text{m}^2$), 2w ($69.76 \pm 1.67 \mu\text{m}^2$), and 4w ($80.05 \pm 2.17 \mu\text{m}^2$). This was in contrast to the nucleus area of diffuse Cath B localization neurons that was approximately $58 \mu\text{m}^2$; 6 h ($71.71 \pm 3.20 \mu\text{m}^2$) $p=1.00$, 1d ($66.84 \pm 1.74 \mu\text{m}^2$) $p=0.02$, 3d ($68.03 \pm 4.03 \mu\text{m}^2$) $p=4.00 \times 10^{-3}$, 1w ($53.64 \pm 3.42 \mu\text{m}^2$) $p=1.48 \times 10^{-10}$, 2w ($41.00 \pm 1.66 \mu\text{m}^2$) $p=3.26 \times 10^{-16}$, and 4w ($46.56 \pm 2.67 \mu\text{m}^2$) $p=1.70 \times 10^{-17}$ (Figure 5D, one-way ANOVA; $F_{11,1303}=29.764$, $p=2.53 \times 10^{-56}$).

Nucleus area had main effects from Cath B localization (two-way ANOVA; $F_{1,1303}=169.495$, $p=1.62 \times 10^{-36}$) and time (two-way ANOVA; $F_{5,1303}=18.102$, $p=2.14 \times 10^{-17}$). Main effects from time and localization were that nucleus area was significantly decreased at most post-injury time points. A significant interaction of Cath B localization and time on nucleus area was also found ($F_{5,1303}=14.462$, $p=8.23 \times 10^{-14}$).

Three-way ANOVA demonstrated significant effects of time ($F_{5,1527}=22.543$, $p=7.15 \times 10^{-22}$), Cath B localization ($F_{1,1527}=104.216$, $p=1.03 \times 10^{-23}$), and membrane disruption ($F_{1,1527}=26.553$, $p=2.90 \times 10^{-7}$) on somal area. Interactions between time and Cath B localization ($F_{5,1527}=2.17$, $p=0.055$) or interactions between membrane disruption

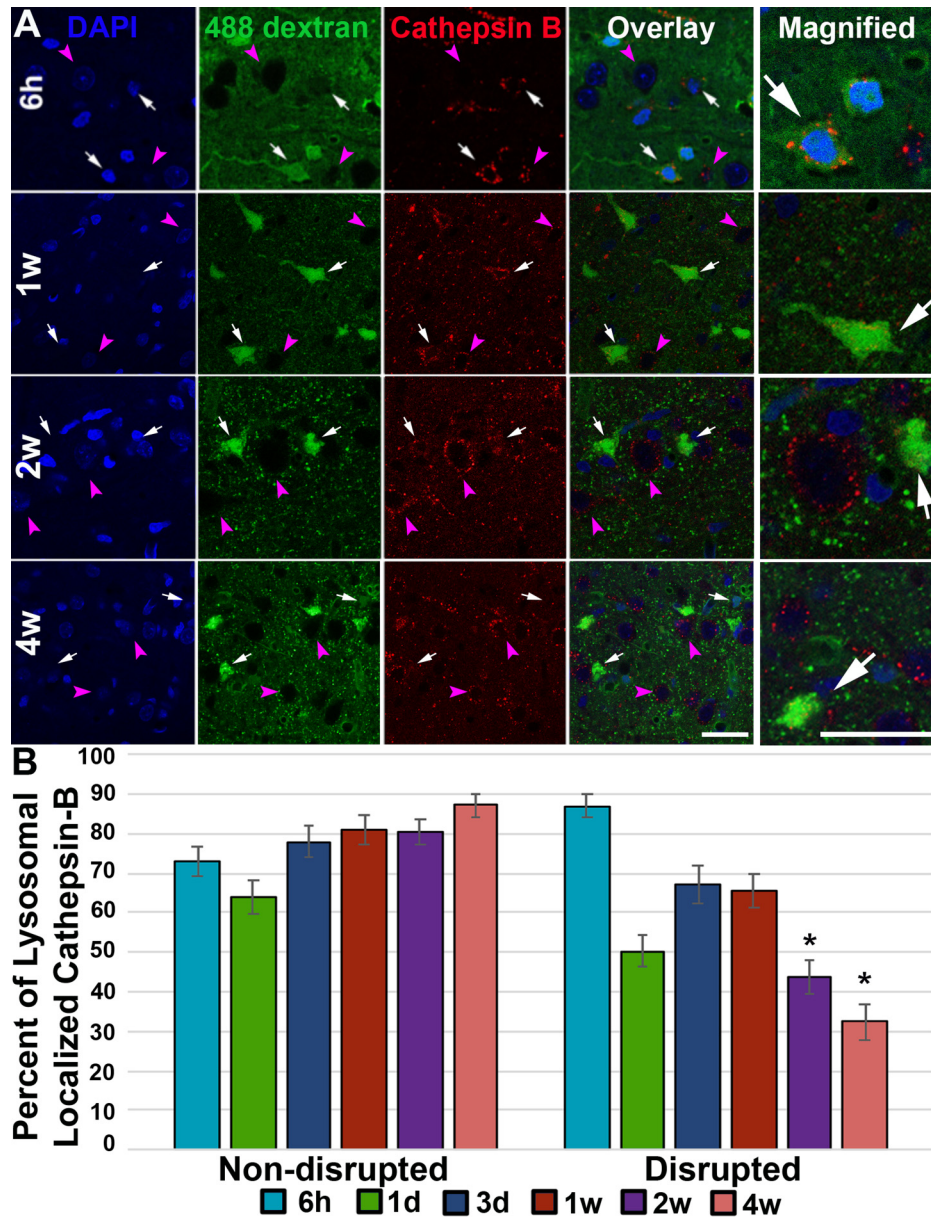


Figure 3. Representative confocal images at 6 h, 1w, 2w, and 4w of immunolabeled Cathepsin B (red) in the lateral neocortex following CFPI (A). Membrane disrupted neurons were identified as containing the cell-impermeable Alexa-488 conjugated dextran (green). The nuclei were labeled with DAPI (blue) to identify the location of non-membrane disrupted neurons. The fourth panel is an overlay, and the last panel is a higher magnification image from the overlay panel. White arrows indicate membrane disrupted neurons and purple arrow heads indicate non membrane disrupted neurons. Scale bar = 20 μ m. Cathepsin B localization shifts in membrane disrupted neurons at 2 and 4w post-CFPI (B). Bar graph depicts the percentage of total analyzed neurons per timepoint with punctate lysosomal cathepsin B localization at 6 h (n = 290 neurons, 5 animals) [teal blue], 1d (n = 282 neurons, 5 animals) [green], 3d (n = 207 neurons, 4 animals) [dark blue], 1w (n = 237 neurons, 5 animals) [red], 2w (n = 300 neurons, 5 animals) [purple], and 4w (n = 235 neurons, 5 animals) [pink] in non-disrupted and membrane disrupted neuronal populations reported as mean \pm S.E.M. * $p < 0.05$.

and Cath B localization alone ($F_{1,1527} = 2.60$, $p = 0.107$) were not significant when assessing soma area using three-way ANOVA. However, interactions between membrane disruption and time were significant ($F_{5,1527} = 2.913$, $p = 0.013$). Additionally, three-way ANOVA demonstrated that there was an interaction of membrane disruption, Cath B

localization, and time post-injury on soma area ($F_{5,1527} = 2.964$, $p = 0.011$).

Main effects from time ($F_{5,1291} = 24.416$, $p = 1.51 \times 10^{-23}$), Cath B localization ($F_{1,1291} = 113.404$, $p = 1.93 \times 10^{-23}$), and membrane disruption ($F_{1,1291} = 80.778$, $p = 8.76 \times 10^{-19}$) on nucleus area were found via three-way ANOVA. There was

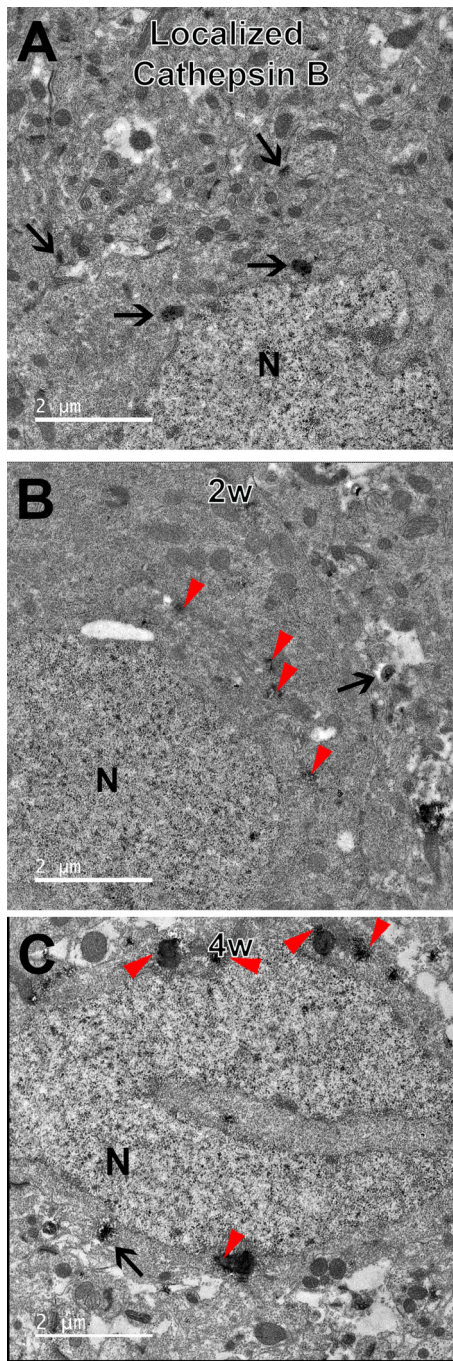


Figure 4. Qualitative ultrastructural confirmation of Cathepsin B redistribution outside of lysosomes following CFPI. Electron micrographs of neurons (“N” indicates the nucleus) immunolabeled for Cath-B (black granules) from a representative 2w and 4w TBI animal. (A) Some neurons in the injured brain displayed normally localized cathepsin B within lysosomes (black arrows). (B & C) Diffuse localization of Cathepsin B outside of the lysosomes (red arrow heads), however, was observed in many of the lateral neocortical neurons in these cases, substantiating the confocal quantitative assessments. Scale bar = 2 μm .

a significant interaction between membrane disruption and Cath B localization on nucleus area ($F_{1,1291} = 15.813$, $p =$

7.40×10^{-5}). Another significant interaction was found between time and membrane disruption ($F_{5,1291} = 9.327$, $p = 9.68 \times 10^{-9}$). An additional significant interaction also noted was between time and Cath B localization ($F_{5,1291} = 6.572$, $p = 5.00 \times 10^{-6}$) on nucleus area. Looking at time, Cath B localization, and membrane disruption as factors for nucleus area did not have a significant interaction as indicated by three-way ANOVA ($F_{5,1291} = 2.187$, $p = 0.053$).

Discussion

In the current study we found no change in the expression of Cath B or any downstream signaling proteins (Bak, Bcl-XL, or AIF) from 6 h to 4w following CFPI in male Sprague Dawley rats compared to shams. While Cath B activity was also unchanged over time following diffuse TBI, Cath B was found to be re-localized into the cytosol in membrane disrupted neurons at 2w and 4w post-injury, a phenomenon not observed in non-membrane disrupted neuron at any time point or membrane disrupted neurons at more acute time points in this study (6 h–1w). Finally, while Hernandez et al. (2019) demonstrated no neuronal loss out to 4w post CFPI, we found indications of neuronal atrophy in relation to membrane disruption and Cath B re-localization throughout the time course, indicating the potential for therapeutic rescue of these pathological populations.

Unlike other Cathepsins, Cath B demonstrates catalytic activity in the cytosol (Pratt et al., 2009). While previous studies assessing a range of neurological damages/diseases report an increase in both expression and activity of Cath B, in the current study, we did not find a change in Cath B protein expression or activity at any time throughout the post-injury time course (6 h–4w) (Foghsgaard et al., 2001; Feldstein et al., 2004; Benchoua et al., 2004; Ellis et al., 2005; Amritraj et al., 2009; Rodríguez-Muela et al., 2015). Our findings are in contrast to what has been observed in previous TBI studies, which indicate an increase in both Cath B protein levels and activity (Luo et al., 2010; Hook et al., 2013; Boutté et al., 2020). Specifically, Luo et al. (2010) analyzed both Cath B activity and expression in the cortex 1–48 h and 7d following CCI and found that Cath B activity increased starting at 6 h increased significantly through 7d compared to sham. This group also quantified Cath B expression which doubled after 6 h, continued to increase until it was increased 4x compared to sham by 48 h. Finally, at 7d, they saw Cath B expression decrease, but still doubled from sham. Hook et al. (2013) evaluated activity and saw a 1.5x increase 2 h post-CCI. Hook et al. also measured protein expression at 24 h post-injury and also found an 4x increase in Cath B expression compared to sham. Another study by Boutté et al. (2020) found an increase in Cath B protein expression following PBBI and demonstrated an increase in Cath B activity at 3d post-injury that remained increased at 7d post-injury, compared to craniotomy alone. However, this increase was not seen at 1d (Boutté et al., 2020).

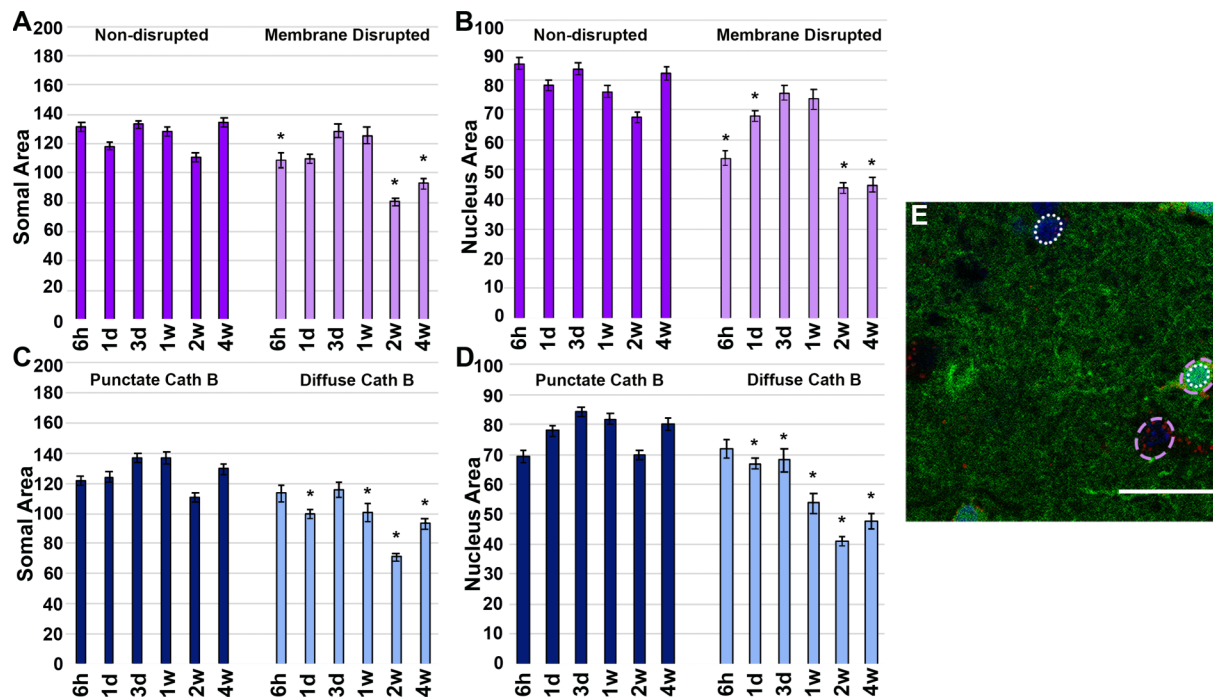


Figure 5. Membrane disruption and Cathepsin B mislocalization affect cell morphology. Bar graphs comparing the mean (A & C) somal area and (B & D) nucleus area 6 h (n = 738 neurons/5 animals), 1 d (n = 527 neurons/5 animals), 3 d (n = 388 neurons/4 animals), 1 w (n = 426 neurons/5 animals), 2 w (n = 577 neurons/ 5 animals), and 4 w (n = 434 neurons/5 animals) following CFPI. These neurons were designated as (A & B) membrane disrupted (light purple bars) and non-disrupted (dark purple bars) or (C & D) based on Cathepsin B localization into puncta (dark blue bars) or diffusely distributed throughout the cytoplasm (light blue bars) in each cell. (E) Representative image indicating somal area (dashed circle) and nucleus area (dotted circle) in a membrane disrupted and non-disrupted neuron at 1 w post-injury. Scale bar = 20 μ m. The area of both the soma and nucleus was decreased in membrane disrupted neurons, and neurons with diffusely localized Cathepsin B. * $p < 0.05$ compared to timepoint-matched internal controls [(A & B) non-membrane disrupted or (C & D) punctate localized Cath B neurons].

The differences between our findings and the findings of the other groups may lie in the circumstances under which these studies were conducted. All of the previous TBI studies utilized injury models that induced a focal homogeneous lesion to the brain (Luo et al., 2010; Hook et al., 2013; Boutté et al., 2020; Sarkar et al., 2020). However, our CFPI model, is a diffuse injury so the nature of the pathologies within the brain in this model are heterogeneous, including the Cath B relocation (Singleton et al., 2002; Singleton and Povlishock, 2004; Lifshitz et al., 2007; Lafrenaye et al., 2012). Therefore, measurement of the entire lateral neocortex Cath B activity may not capture the cells that could exhibit increased Cath B expression. Also, in combination with different modalities of injury and consideration of the variance in pathology, the timeframes in which Cath B was assessed in the previous studies were acute and sub-acute, juxtaposed to our sub-acute and late timepoints. The results from those works and ours suggest that Cath B activity and protein expression could be time and pathology dependent.

In the current study we also found relocation of Cath B that appears to be associated with neuronal membrane

disruption post-CFPI. This observation of Cath B outside of the lysosomes could indicate neurons undergoing lysosomal membrane permeabilization (LMP). Brain injury-induced organelle membrane disruption, such as LMP, involving the Cath B pathway has been previously observed (Windelborn and Lipton, 2008; Oberle et al., 2010; Luo et al., 2010; Kilinc et al., 2010; Rodríguez-Muela et al., 2015; Meyer et al., 2021). Pathological findings of LMP indicate progression to cell death; however, there is no previous observation of cell death in the CFPI animals (Hernandez et al., 2019). A possibility for the release of Cath B through LMP includes cytosolic phospholipase A2 (cPLA2). Studies looking at the role of other Cathepsins (D and L) in neurotrauma autophagy found that cPLA2 is directly involved in LMP in mice and that these sequelae involve the release of lysosomal enzymes (Li et al., 2019; Sarkar et al., 2020). cPLA2 has also been proposed to alter the neuronal plasma membrane (Lee et al., 2011). Therefore, cPLA2 could be disrupting the lysosomal membrane inducing the release of Cath B into the cytosol and also targeting the plasma membrane. Additionally, disruption of the lysosomes or replacement of Cath B with Cath L impedes neurite outgrowth. Cath B has

been shown to remodel neurites in vitro through lysosomal membrane trafficking (Jiang et al., 2020). Perhaps the release of Cath B dysregulates plasma membrane remodeling through disruption of lysosomal function thus could be why membrane disruption is evident at later time points.

Work looking at 6 h post-CFPI with intracranial pressure elevation highlighted that Cath B relocalizes from the lysosomal compartments into the cytosol in membrane disrupted neurons (Lafrenaye et al., 2012). In this study, however, Cath B relocalization was significant in the 2w and 4w groups, particularly in the membrane disrupted neurons, but not at 6 h, even in the membrane disrupted neuronal population. Fisher rats were used in the Lafrenaye et al. (2012) study while the current study used Sprague Dawley rats, indicating that there could be strain difference that may exacerbate Cath B release from the lysosomes, as observed in our prior study. Furthermore, the majority of the animals evaluated for Cath B relocalization in the 2012 study had both a CFPI and elevated ICP. That group had also found ICP elevation exacerbates membrane disruption and causes cell loss at 4w (Lafrenaye et al., 2014), the combination of TBI and secondary ICP elevations may induce more severe Cath B relocalization, however, further assessments of this possibility are needed.

Finally, we found that while somal and nuclear area were consistent for non-membrane disrupted neurons and neurons demonstrating lysosomal-Cath B, neurons sustaining later stage membrane disruption or Cath B redistribution, had significantly smaller soma and nuclei, indicating atrophy. This atrophy occurred simultaneously with the resurgence of membrane disruption and Cath B relocalization found at the later post-injury time points of 2w and 4w. Interestingly, no difference was observed in the somal and nucleus areas between the non-disrupted and membrane disrupted neuronal populations at 3d and 1w, unlike the significant reductions seen acutely (6 h–1d) and at later time points (2w–4w) following TBI. These observations are in accordance with the previous findings in Hernandez et al. (2019), that neuronal membrane disruption appears to be biphasic following CFPI. Additionally, Hernandez et al. (2019) found that 6 h–4w post-CFPI animals did not feature neuronal loss nor evidence of cell death, supporting the idea that these atrophying neurons may be rescuable. Atrophy without concomitant cell death has also been observed by other groups following CFPI (Lifshitz et al., 2007; Greer et al., 2011), further corroborating this idea. This weeks-long therapeutic window of atrophy without cell death, provides an opportunity to salvage these membrane disrupted and Cath B relocalized neurons. Particularly, future studies focused on pharmacologically targeting Cath B for the recovery of the membrane disrupted neuronal population are warranted.

Overall, our study found that Cath B is being re-distributed into the cytosol, notably within the membrane disrupted neuron subpopulation. Moreover, these membrane disrupted neurons significantly present Cath B relocalization late (2w–

4w) following injury and the Hernandez et al. (2019) study highlighted that these neurons are not dying. While these Cath B relocalized neurons are not dying, they demonstrate both membrane disruption and atrophy. Both observations are indicative of a late secondary pathology and there is opportunity for therapeutic treatment of these neurons in diffuse TBI.

Abbreviations

TBI	Traumatic brain injury
Cath B	Cathepsin B
h	hours
w	weeks
Bcl-2	B-cell lymphoma 2
AIF	apoptosis initiating factor
CCI	controlled cortical impact
PBBI	penetrating ballistic-like brain injury
CFPI	central fluid percussion injury
ICP	intracranial pressure
HRP	horseradish peroxidase
DAPI	4',6-diamidino-2-phenylindole
BSA	bovine serum albumin
DTT	dithiothreitol
EDTA	Ethylenediaminetetraacetic acid
ZFR-AMC	Z-Phe-Arg-7-amino-4-(trifluoromethyl) coumarin
EM	electron microscopy
ANOVA	analysis of variance
LMP	lysosomal membrane permeabilization
cPLA2	cytosolic phospholipase 2.

Acknowledgments

The authors would like to recognize Judy Williamson, Frances White, Susan Walker, and Nicole Welborn for invaluable assistance. This work was supported by NINDS grant 1R01NS096143. Microscopy was performed at the VCU Department of Anatomy and Neurobiology Microscopy Facility, supported, in part, with funding from NIH-NINDS Center core grant 5P30NS047463 and with funding from NIH-NCI Cancer Center Support Grant (P30CA016059).

Authors' Contribution

MLH carried out the confocal microscopic and ultrastructural analyses, western and protein activity assessments, and wrote the manuscript. MM and KMG carried out the confocal analyses and western assessments. ADL carried out the confocal microscopic analyses and western assessments, conceived, designed and coordinated the study, and wrote the manuscript.

Declaration of conflicting interests


The author(s) declared no potential conflicts of interest with respect to the research, authorship, and/or publication of this article.

Funding

The author(s) disclosed receipt of the following financial support for the research, authorship, and/or publication of this article: This work was supported by the NINDS grant 1R01NS096143. Microscopy was performed at the VCU Department of Anatomy and

Neurobiology Microscopy Facility, supported, in part, with funding from NIH-NINDS Center core grant 5P30NS047463 and with funding from NIH-NCI Cancer Center Support Grant (P30CA016059).

ORCID iD

Martina L. Hernandez  <https://orcid.org/0000-0001-7337-4271>

Supplemental material

Supplemental material for this article is available online.

References

- Amritraj, A., Peake, K., Kodam, A., Salio, C., Merighi, A., Vance, J. E., & Kar, S. (2009). Increased activity and altered subcellular distribution of lysosomal enzymes determine neuronal vulnerability in Niemann-Pick type C1-deficient mice. *The American Journal of Pathology*, *175*(6), 2540–2556. <https://doi.org/10.2353/ajpath.2009.081096>
- Benchoua, A., Braudeau, J., Reis, A., Couriaud, C., & Onténiente, B. (2004). Activation of proinflammatory caspases by cathepsin B in focal cerebral ischemia. *Journal of Cerebral Blood Flow & Metabolism*, *24*(11), 1272–1279. <https://doi.org/10.1097/01.WCB.0000140272.54583.FB>
- Boutté, A. M., Hook, V., Thangavelu, B., Sarkis, G. A., Abbatiello, B. N., Hook, G., Jacobsen, J. S., Gilsdorf, J., Yang, Z., Wang, K. K. W., & Shear, D. A. (2020). Penetrating traumatic brain injury triggers dysregulation of Cathepsin B protein levels independent of cysteine protease activity in brain and cerebral spinal fluid. *Journal of Neurotrauma*, *37*(13), 1574–1586. <https://doi.org/10.1089/neu.2019.6537>
- Boya, P., Andraeu, K., Poncet, D., Zamzami, N., Perfettini, J. L., Metivier, D., Ojcius, D. M., Jäättelä, M., & Kroemer, G. (2003). Lysosomal membrane permeabilization induces cell death in a mitochondrion-dependent fashion. *Journal of Experimental Medicine*, *197*(10), 1323–1334. <https://doi.org/10.1084/jem.20021952>
- Cavallo-Medved, D., Moin, K., & Sloane, B. (2011). Cathepsin B: basis sequence: mouse. *AFCS-nature Molecule Pages*, *2011*, 1–17. PMID: PMC5541861
- Chaitanya, G. V., & Babu, P. P. (2008). Multiple apoptogenic proteins are involved in the nuclear translocation of apoptosis inducing factor during transient focal cerebral ischemia in rat. *Brain Research*, *1246*, 178–190. <https://doi.org/10.1016/j.brainres.2008.09.075>
- Chowdhury, K. D., Sarkar, A., Chatterjee, S., Patra, D., Sengupta, D., Banerjee, S., Chakraborty, P., & Sadhukhan, G. C. (2019). Cathepsin B mediated scramblase activation triggers cytotoxicity and cell cycle arrest by andrographolide to overcome cellular resistance in cisplatin resistant human hepatocellular carcinoma HepG2 cells. *Environmental Toxicology and Pharmacology*, *68*, 120–132. <https://doi.org/10.1016/j.etap.2019.03.003>
- de Castro, M., Bunt, G., & Wouters, F. (2016). Cathepsin B launches an apoptotic exit effort upon cell death-associated disruption of lysosomes. *Cell Death Discovery*, *2*(1), 16012. <https://doi.org/10.1038/cddiscovery.2016.12>
- Dixon, C. E., Lyeth, B. G., Povlishock, J. T., Findling, R. L., Hamm, R. J., Marmarou, A., Young, H. F., & Hayes, R. L. (1987). A fluid percussion model of experimental brain injury in the rat. *Journal of Neurosurgery*, *67*(1), 110–119. <https://doi.org/10.3171/jns.1987.67.1.0110>
- Ellis, R. C., O’Steen, W. A., Hayes, R. L., Nick, H. S., Wang, K. K. W., & Anderson, D. K. (2005). Cellular localization and enzymatic activity of cathepsin B after spinal cord injury in the rat. *Experimental Neurology*, *193*(1), 19–28. <https://doi.org/10.1016/j.expneurol.2004.11.034>
- Feldstein, A. E., Werneburg, N. W., Canbay, A., Guicciardi, M. E., Bronk, S. F., Rydzewski, R., Burgart, L. J., & Gores, G. J. (2004). Free fatty acids promote hepatic lipotoxicity by stimulating TNF- α expression via a lysosomal pathway. *Hepatology*, *40*(1), 185–194. <https://doi.org/10.1002/hep.20283>
- Foghsgaard, L., Wissing, D., Mauch, D., Lademann, U., Bastholm, L., Boes, M., Elling, F., Leist, M., & Jäättelä, M. (2001). Cathepsin B acts as a dominant execution protease in tumor cell apoptosis induced by tumor necrosis factor. *Journal of Cell Biology*, *153*(5), 999–1009.
- Greer, J. E., McGinn, M. J., & Povlishock, J. T. (2011). Diffuse traumatic axonal injury in the mouse induces atrophy, c-Jun activation, and axonal outgrowth in the axotomized neuronal population. *Journal of Neuroscience*, *31*(13), 5089 LP – 5105. <https://doi.org/10.1523/JNEUROSCI.5103-10.2011>
- Hernandez, M. L., Chatlos, T., Gorse, K. M., & Lafrenaye, A. D. (2019). Neuronal membrane disruption occurs late following diffuse brain trauma in rats and involves a subpopulation of NeuN negative cortical neurons. *Frontiers in Neurology*, *10*. <https://doi.org/10.3389/fneur.2019.01238>
- Hook, G. R., Yu, J., Sipes, N., Pierschbacher, M. D., Hook, V., & Kindy, M. S. (2013). The cysteine protease cathepsin B is a key drug target and cysteine protease inhibitors are potential therapeutics for traumatic brain injury. *Journal of Neurotrauma*, *31*(5), 515–529. <https://doi.org/10.1089/neu.2013.2944>
- Jiang, M., Meng, J., Zeng, F., Qing, H., Hook, G., Hook, V., Wu, Z., & Ni, J. (2020). Cathepsin B inhibition blocks neurite outgrowth in cultured neurons by regulating lysosomal trafficking and remodeling. *Journal of Neurochemistry*, *155*(3), 300–312. <https://doi.org/10.1111/jnc.15032>
- Keating, C. E., Browne, K. D., Duda, J. E., & Cullen, D. K. (2020). Neurons in subcortical oculomotor regions are vulnerable to plasma membrane damage after repetitive diffuse traumatic brain injury in swine. *Journal of Neurotrauma*, *37*(17), 1918–1932. <https://doi.org/10.1089/neu.2019.6738>
- Khouri, H. E., Plouffe, C., Hasnain, S., Hiramata, T., Storer, A. C., & Menard, R. (1991). A model to explain the pH-dependent specificity of cathepsin B-catalysed hydrolyses. *Biochemical Journal*, *275*(3), 751–757. <https://doi.org/10.1042/bj2750751>
- Kilinc, M., Gürsoy-Özdemir, Y., Gürer, G., Erdener, S. E., Erdemli, E., Can, A., & Dalkara, T. (2010). Lysosomal rupture, necroapoptotic interactions and potential crosstalk between cysteine proteases in neurons shortly after focal ischemia. *Neurobiology of Disease*, *40*(1), 293–302. <https://doi.org/10.1016/j.nbd.2010.06.003>
- Lafrenaye, A. D., Krahe, T. E., & Povlishock, J. T. (2014). Moderately elevated intracranial pressure after diffuse traumatic brain injury is associated with exacerbated neuronal pathology and behavioral morbidity in the rat. *Journal of Cerebral Blood Flow & Metabolism*, *34*(10), 1628–1636. <https://doi.org/10.1038/jcbfm.2014.122>
- Lafrenaye, A. D., McGinn, M. J., & Povlishock, J. T. (2012). Increased intracranial pressure after diffuse traumatic brain

- injury exacerbates neuronal somatic membrane poration but not axonal injury: evidence for primary intracranial pressure-induced neuronal perturbation. *Journal of Cerebral Blood Flow & Metabolism*, 32(10), 1919–1932. <https://doi.org/10.1038/jcbfm.2012.95>
- LaPlaca, M. C., Lessing, M. C., Prado, G. R., Zhou, R., Tate, C. C., Geddes-Klein, D., Meaney, D. F., & Zhang, L. (2019). Mechanoporation is a potential indicator of tissue strain and subsequent degeneration following experimental traumatic brain injury. *Clinical Biomechanics*, 64, 2–13. <https://doi.org/10.1016/j.clinbiomech.2018.05.016>
- Lee, J. C. M., Simonyi, A., Sun, A. Y., & Sun, G. Y. (2011). Phospholipases A2 and neural membrane dynamics: implications for Alzheimer's disease. *Journal of Neurochemistry*, 116(5), 813–819. <https://doi.org/10.1111/j.1471-4159.2010.07033.x>
- Li, Y., Jones, J. W., Choi, H., Sarkar, C., Kane, M. A., Koh, E. Y., Lipinski, M. M., & Wu, J. (2019). cPLA2 activation contributes to lysosomal defects leading to impairment of autophagy after spinal cord injury. *Cell Death & Disease*, 10(7), 531. <https://doi.org/10.1038/s41419-019-1764-1>
- Lifshitz, J., Kelley, B. J., & Povlishock, J. T. (2007). Perisomatic thalamic axotomy after diffuse traumatic brain injury is associated with atrophy rather than cell death. *Journal of Neuropathology and Experimental Neurology*, 66(3), 218–229. <https://doi.org/10.1097/01.jnen.0000248558.75950.4d>
- Luo, C. L., Chen, X. P., Yang, R., Sun, Y. X., Li, Q. Q., Bao, H. J., Cao, Q. Q., Ni, H., Qin, Z. H., & Tao, L. Y. (2010). Cathepsin B contributes to traumatic brain injury-induced cell death through a mitochondria-mediated apoptotic pathway. *Journal of Neuroscience Research*, 88(13), 2847–2858. <https://doi.org/10.1002/jnr.22453>
- Marin, J. R., Weaver, M. D., & Mannix, R. C. (2017). Burden of USA hospital charges for traumatic brain injury. *Brain Inj.*, 31(1), 24–31. <https://doi.org/10.1080/02699052.2016.1217351>
- McMahon, P., Hricik, A., Yue, J. K., Puccio, P. M., Inoue, T., Lingsma, H. F., Beers, S. R., Gordon, W. A., Valadka, A. B., Manley, G. T., Okonkwo, D. O. and the TRACK-TBI investigators including, Casey, S. S., Cooper, S. R., Dams-O'Connor, K., Menon, D. K., Sorani, M. D., Yuh, E. L., Mukherjee, P., Schnyer, D. M., & Vassar, M. J. (2014). Symptomatology and functional outcome in mild traumatic brain injury: Results from the prospective TRACK-TBI study. *J. Neurotrauma*, 31(1), 26–33. <https://doi.org/10.1089/neu.2013.2984>
- Meyer, N., Henkel, L., Linder, B., Zielke, S., Tascher, G., Trautmann, S., & Geisslinger, G., Münch, C., Fulda, S., Tegeder, I., & Kögel, D. (2021). Autophagy activation, lipotoxicity and lysosomal membrane permeabilization synergize to promote pimozone- and loperamide-induced glioma cell death. *Autophagy*, 17(11), 3424–3443. <https://doi.org/10.1080/15548627.2021.1874208>
- Mollan, S. P., Ali, F., Hassan-Smith, G., Botfield, H., Friedman, D. I., & Sinclair, A. J. (2016). Evolving evidence in adult idiopathic intracranial hypertension: pathophysiology and management. *Journal of Neurology, Neurosurgery & Psychiatry*, 87(9), 982–992. <https://doi.org/10.1136/jnnp-2015-311302>
- Nagakannan, P., Islam, I., Conrad, M., Eftekharpour, E., Islam, M. I., Conrad, M., & Eftekharpour, E. (2021). Cathepsin B is an executor of ferroptosis. *BBA – Molecular Cell Research*, 1868(3), 118928. <https://doi.org/10.1016/j.bbamcr.2020.118928>
- Nägler, D. K., Storer, A. C., Portaro, F. C. V., Carmona, E., Juliano, L., & Ménard, R. (1997). Major increase in endopeptidase activity of human cathepsin B upon removal of occluding loop contacts. *Biochemistry*, 36(41), 12608–12615. <https://doi.org/10.1021/bi971264+>
- Oberle, C., Huai, J., Reinheckel, T., Tacke, M., Rassner, M., Ekert, P. G., Buellesbach, J., & Borner, C. (2010). Lysosomal membrane permeabilization and cathepsin release is a bax/bak-dependent, amplifying event of apoptosis in fibroblasts and monocytes. *Cell Death & Differentiation*, 17(7), 1167–1178. <https://doi.org/10.1038/cdd.2009.214>
- Prado, G. R., & LaPlaca, M. C. (2020). Neuronal plasma membrane integrity is transiently disturbed by traumatic loading. *Neuroscience Insights*, 15, 263310552094609. <https://doi.org/10.1177/2633105520946090>
- Pratt, M. R., Sekedat, M. D., Chiang, K. P., & Muir, T. W. (2009). Direct measurement of Cathepsin B activity in the cytosol of apoptotic cells by an activity-based probe. *Chemistry & Biology*, 16(9), 1001–1012. <https://doi.org/10.1016/j.chembiol.2009.07.011>
- Rodríguez-Muela, N., Hernández-Pinto, A. M., Serrano-Puebla, A., García-Ledo, L., Latorre, S. H., La Rosa, E. J. De, & Boya, P. (2015). Lysosomal membrane permeabilization and autophagy blockade contribute to photoreceptor cell death in a mouse model of retinitis pigmentosa. *Cell Death & Differentiation*, 22(3), 476–487. <https://doi.org/10.1038/cdd.2014.203>
- Ruzza, P., Quintieri, L., Osler, A., Calderan, A., Biondi, B., Floreani, M., Guiotto, A., & Borin, G. (2006). Fluorescent, internally quenched, peptides for exploring the pH-dependent substrate specificity of cathepsin B. *Journal of Peptide Science*, 12(7), 455–461. <https://doi.org/10.1002/psc.748>
- Ryu, J., Stone, P., Lee, S., Payne, B., Gorse, K., & Lafrenaye, A. (2021). Buprenorphine alters microglia and astrocytes acutely following diffuse traumatic brain injury. *Scientific Reports*, 11(1), 8620. <https://doi.org/10.1038/s41598-021-88030-z>
- Sarkar, C., Jones, J. W., Hegdekar, N., Thayer, J. A., Kumar, A., Faden, A. I., Kane, M. A., & Lipinski, M. M. (2020). PLA2G4A/cPLA2-mediated Lysosomal membrane damage leads to inhibition of autophagy and neurodegeneration after brain trauma. *Autophagy*, 16(3), 466–485. <https://doi.org/10.1080/15548627.2019.1628538>
- Singleton, R. H., & Povlishock, J. T. (2004). Identification and characterization of heterogeneous neuronal injury and death in regions of diffuse brain injury: evidence for multiple independent injury phenotypes. *Journal of Neuroscience*, 24(14), 3543–3553. <https://doi.org/10.1523/JNEUROSCI.5048-03.2004>
- Singleton, R. H., Zhu, J., Stone, J. R., & Povlishock, J. T. (2002). Traumatically induced axotomy adjacent to the soma does not result in acute neuronal death. *The Journal of Neuroscience*, 22(3), 791 LP – 802. <https://doi.org/10.1523/JNEUROSCI.22-03-00791.2002>
- Taylor, C. A., Bell, J. M., Breiding, M. J., & Xu, L. (2017). Traumatic brain injury–related emergency department visits, hospitalizations, and deaths — United States, 2007 and 2013. *MMWR. Surveill. Summ.*, 66(9), 1–16. <https://doi.org/10.15585/mmwr.ss6609a1>
- Windelborn, J. A., & Lipton, P. (2008). Lysosomal release of cathepsins causes ischemic damage in the rat hippocampal slice and depends on NMDA-mediated calcium influx, arachidonic acid

- metabolism, and free radical production. *Journal of Neurochemistry*, *106*(1), 56–69. <https://doi.org/10.1111/j.1471-4159.2008.05349.x>
- Yoon, M. C., Solania, A., Jiang, Z., Christy, M. P., Podvin, S., Mosier, C., Lietz, C. B., Ito, G., Gerwick, W. H., Wolan, D. W., Hook, G., Donoghue, A. J., & Hook, V. (2021). Selective neutral pH inhibitor of Cathepsin B designed based on cleavage preferences at cytosolic and lysosomal pH conditions. *ACS Chemical Biology*, *16*(9), 1628–1643. <https://doi.org/10.1021/acscchembio.1c00138>